Multigap superconductivity in ThAsFeN investigated using μSR measurements

Devashibhai Adroja,[1,2,*] Amitava Bhattacharyya,[1,3,†] Pabitra Kumar Biswas,[1] Michael Smidman,[4] Adrian D. Hillier,[1] Huican Mao,[5] Huiqian Luo,[5] Guang-Han Cao,[6] Zhicheng Wang,[6] and Cao Wang[7]

[1]*ISIS Facility, Rutherford Appleton Laboratory, Chilton, Didcot Oxon OX11 0QX, United Kingdom*

[2]*Highly Correlated Matter Research Group, Physics Department, University of Johannesburg, P.O. Box 524, Auckland Park 2006, South Africa*

[3]*Department of Physics, Ramakrishna Mission Vivekananda University, Howrah 711202, India*

[4]*Center for Correlated Matter and Department of Physics, Zhejiang University, Hangzhou 310058, China*

[5]*Beijing National Laboratory for Condensed Matter Physics, Institute of Physics, Chinese Academy of Sciences, Beijing 100190, China*

[6]*Department of Physics, State Key Laboratory of Silicon Materials, Zhejiang University, Hangzhou 310027, China*

[7]*Department of Physics, Shandong University of Technology, Zibo 255049, China*

(Received 9 June 2017; revised manuscript received 11 September 2017; published 3 October 2017)

We have investigated the superconducting ground state of the newly discovered superconductor ThFeAsN with a tetragonal layered crystal structure using resistivity, magnetization, heat capacity, and transverse-field muon-spin rotation (TF-μSR) measurements. Our magnetization and heat-capacity measurements reveal an onset of bulk superconductivity with $T_c \sim 30$ K. A nonlinear magnetic-field dependence of the specific heat coefficient $\gamma(H)$ has been found in the low-temperature limit, which indicates that there is a nodal energy gap. Our analysis of the TF-μSR results shows that the temperature dependence of the superfluid density is better described by a two-gap model either isotropic $s+s$ wave or $s+d$ wave than a single-gap isotropic s-wave model for the superconducting gap, consistent with other Fe-based superconductors. The combination of $\gamma(H)$ and TF-μSR results suggest that the $(s+d)$-wave model is the most consistent candidate for the gap structure of ThFeAsN. The observation of two gaps in ThFeAsN suggests a multiband nature of the superconductivity possibly arising from the d bands of Fe ions. Furthermore, from our TF-μSR study we have estimated the magnetic penetration depth in the polycrystalline sample of $\lambda_L(0) = 375$ nm, superconducting carrier density $n_s = 4.97\times10^{27}$ m^{-3}, and carrier's effective-mass $m^* = 2.48m_e$. We compare the results of our present paper with those reported for the Fe-pnictide families of superconductors.

DOI: 10.1103/PhysRevB.96.144502

I. INTRODUCTION

In a conventional superconductor, the binding of electrons into the paired states, known as Cooper pairs, is responsible for superconductivity as described in the Bardeen-Cooper-Schrieffer (BCS) theory in 1957 [1]. However, the BCS theory often fails to describe the superconductivity (SC) observed in strongly correlated materials. Several strongly correlated superconducting materials, having magnetic f- or d-electron elements, exhibit unconventional SC, and various theoretical models based on magnetic interactions (magnetic glue) and spin fluctuations have been proposed to understand these superconductors [2,3]. Gauge symmetry is broken in the case of conventional BCS superconductors, and for this, other symmetries of the Hamiltonian are broken for unconventional superconductors in the superconducting state. BCS superconductors also can show gap anisotropy, although they remain nodeless and the gap does not change sign over the Fermi surface, whereas unconventional superconductors may have nodes (zeros) in the gap function along certain directions, and the location of the nodes is closely associated with the pairing symmetry. Therefore investigation of the superconducting gap structure of strongly correlated f- and d-electron superconductors is very important for understanding the physics of unconventional pairing mechanisms in these classes of materials.

Unconventional superconductivity has been observed in high-temperature cuprates [4], iron pnictides [5], and heavy fermion materials [6], which have strong electronic correlations and quasi-two dimensionality. Interestingly superconductivity in the iron-based materials emerges after doping electrons/holes into an antiferromagnetic parent compound [5], for example, $LaFeAsO_{1-x}F_x$ (1111 family) [7,8], $BaFe_{2-x}Co_xAs_2$ (122 family) [9], $NaFe_{1-x}Co_xAs$ (111 family) [10], $FeTe_{1-x}Se_x$ (11 family) [11,12], and $Ca_{1-x}La_xFeAs_2$ (112 family) [13,14], etc. Some special systems are self-doped by the ion deficiency, such as $LaFeAsO_{1-\delta}$ [15] and $Li_{1-\delta}FeAs$ [16]. It is interesting that, in the 1111 family of Fe-based materials, superconductivity can be induced by chemical substitution (i.e., electron and hole doping) on any atomic site, for example, an antiferromagnetically ordered ground state in LaFeAsO is transformed into a superconducting ground state with fluorine and hydride doping on the oxygen site (e.g., $LaFeAsO_{1-x}F_x$, $LaFeAsO_{1-x}H_x$) [17–20].

It is of great interest to explore possible unconventional superconductivity in stoichiometric Fe-based layered materials, having tetragonal crystal structures with significant electron correlations. Recently, the first nitride iron pnictide superconductor ThFeAsN, containing layers with nominal compositions $[Th_2N_2]$ and $[Fe_2As_2]$ (the inset of Fig. 1), has been discovered with $T_c = 30$ K for the nominally undoped compound [21]. The transition temperature of this newly discovered

*devashibhai.adroja@stfc.ac.uk

†amitava.bhattacharyya@rkmvu.ac.in

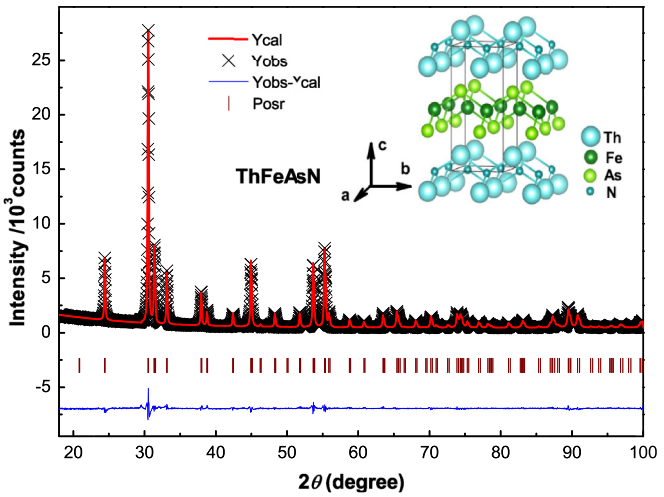

FIG. 1. X-ray powder-diffraction pattern (at 300 K) with the Rietveld refinement fit of the data of ThFeAsN. The line drawn through the data points corresponds to the calculated pattern, and the cross symbols represent observed data. The vertical bars show the Bragg peaks' positions, and the blue line at the bottom shows the difference plot. The inset shows the tetragonal crystal structure [26].

material is as high as the electron-doped 1111-based superconductors and another family of newly discovered stoichiometric superconductors $ACa_2Fe_4As_4F_2$ (A = K, Rb, and Cs, $T_c \sim 30$ K) [22,23]. Although the first-principles calculations of ThFeAsN indicate that the lowest-energy magnetic ground state is the stripe-type antiferromagnetic state [24,25], the normal-state resistivity shows no obvious magnetic anomaly but only metallic behavior down to 30 K [21]. The electron doping by substituting N with O or hole doping by substituting Th with Y only suppresses the superconducting T_c. The density functional theory calculations of ThFeAsN show approximately nested hole and electron Fermi surfaces of Fe d character involving the xz, yz, and xy orbitals, indicating strong similarity to the other Fe-pnictide families of superconductors [24,25]. ThFeAsN shares similar electronic structures and magnetic properties with those of LaOFeAs [25]. The calculated bare susceptibility $\chi_0(\mathbf{q})$ of ThFeAsN peaks at the M point, suggesting perfect nesting between the holelike and the electronlike Fermi surfaces with vector $\mathbf{q} = (\pi,\pi,0)$, similar to other FeAs-based superconductors [25]. Furthermore, the nonmagnetic ground state of ThFeAsN down to 2 K has been confirmed by powder neutron-diffraction measurements [26] and a ^{57}Fe Mössbauer spectroscopy study on polycrystalline samples [27].

In addition to all the existing information, it is important to understand the superconducting and magnetic properties of ThFeAsN on a microscopic level. Transverse-field muon-spin rotation (TF-μSR) and relaxation measurements provide direct information on the nature of the superconducting gap symmetry and absolute value of the magnetic penetration depth. We therefore have investigated the superconducting properties of ThFeAsN using the bulk properties and TF-μSR measurements. Our study of the TF-μSR shows that the temperature dependence of the superfluid density is better described by a two-gap $(s+s)$- or $(s+d)$-wave model than a single-gap isotropic s-wave model.

II. EXPERIMENTAL DETAILS

A polycrystalline sample of ThFeAsN was synthesized by the solid-state reaction method as described by Wang *et al.* [21]. The sample was characterized using powder x-ray diffraction, electrical resistivity, magnetic susceptibility, and heat-capacity measurements. The resistivity and heat capacity were measured using a Quantum Design physical property measurement system between 1.5 and 300 K. Temperature-dependent resistivity from 2 to 300 K was measured by a standard four-probe method. The heat capacity was measured using a standard thermal relaxation method with a sample of $m = 18$ mg. The dc magnetization of the same sample was measured on a Quantum Design magnetic property measurement system. μSR experiments were carried out in the MUSR spectrometer at the ISIS pulsed muon source of the Rutherford Appleton Laboratory, United Kingdom [28]. The μSR measurements were performed in TF mode. A pellet (12-mm diameter) of polycrystalline ThFeAsN was mounted on a silver (99.999%) sample holder. Hematite (α-Fe_2O_3) slabs were placed just after the sample to reduce the background signal. The sample was cooled under He-exchange gas in a He-4 cryostat operating in the temperature range of 1.5–300 K. TF-μSR experiments were performed in the superconducting mixed state in an applied field of 400 G, well above the lower critical field of $H_{c1} \sim$ 30 G of this material. Data were collected in the field-cooled (FC) mode where the magnetic field was applied above the superconducting transition temperature and the sample was then cooled down to base temperature. Muon-spin rotation and relaxation is a dynamic method that allows one to study the nature of the pairing symmetry in superconductors [29]. The vortex state in the case of type-II superconductors gives rise to a spatial distribution of local magnetic fields; which demonstrates itself in the μSR signal through a relaxation of the muon polarization. The data were analyzed using the free software package WIMDA [30].

III. RESULTS AND DISCUSSIONS

The analysis of the powder x-ray diffraction at 300 K reveals that the sample is single phase and crystallizes in the ZrCuSiAs-type tetragonal crystal structure with space-group $P4/nmm$ (No. 129, $Z = 2$) as shown in the inset of Fig. 1. The refined values of the lattice parameters are $a = 4.0367(2)$ and $c = 8.5262(2)$ Å. The layered structure of ThFeAsN is shown in the inset of Fig. 1 perpendicular to the c axis where separated layers of Th and N ions at the bottom and top of the unit cell (along the c axis) can be seen. The As and Fe layers are halfway along the c axis. The Fe and As ions form tetrahedrons with two As-Fe-As bond angles $\alpha \sim 107.0^\circ$ and $\beta \sim 114.5^\circ$ at 300 K. The layered structure of ThFeAsN is very similar to others in the 1111 family of iron pnictide superconductors [15].

The electrical resistivity reveals a sharp drop below 30 K followed by zero resistivity indicating the onset of superconductivity with $T_c = 30$ K [Fig. 2(a)]. In the zero field, the temperature-dependent resistivity of ThFeAsN is metallic and exhibits a power-law behavior $\rho = \rho_0 + aT^n$ with $n \sim 1.3$ between T_c and 150 K, indicating non-Fermi-liquid behavior [26]. The low-field magnetic susceptibility measured in an applied field of 5 G shows an onset of diamagnetism below

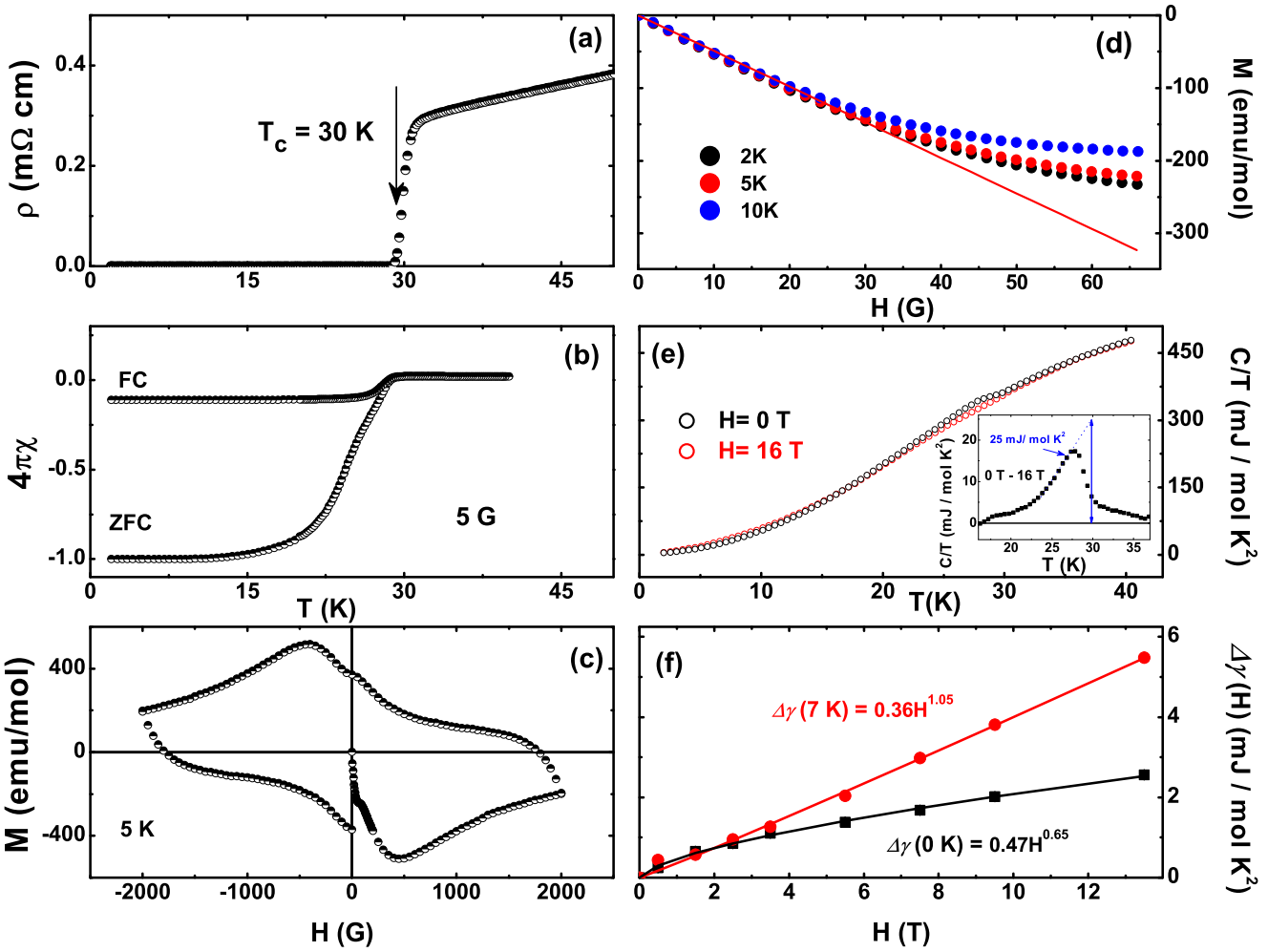

FIG. 2. (a) Temperature dependence of electrical resistivity, (b) Low-field dc-magnetic susceptibility measured in zero-field cooled (ZFC) and FC modes in an applied field of 5 G. (c) The isothermal field dependence of magnetization at 5 K. (d) The isothermal field dependence of magnetization at low field at 2, 5, and 10 K. (e) Temperature dependence of the heat capacity divided by temperature in a zero field and in an applied field of 16 T, and the inset shows the difference of the heat-capacity data 0–16 T plotted as C/T vs T. The blue vertical arrow shows the jump in C/T at T_c. (f) The magnetic-field dependence of the electronic specific heat coefficient $\Delta\gamma$ [$= \gamma(H) - \gamma(0)$] extrapolated to $T \sim 0$ and 7 K. The solid lines show a power-law fit $\gamma(H) \sim H^n$.

30 K indicating that the superconductivity occurs at 30 K and the superconducting volume fraction is close to 100% at 5.0 K [Fig. 2(b)]. This result confirms the bulk nature of superconductivity with $T_c = 30$ K in ThFeAsN, which is comparable to $T_c = 26$ K observed in fluorine-doped LaFeAsO [31]. Very similar behavior of the resistivity and magnetic susceptibility has been reported for ThFeAsN by Mao *et al.* [26].

The magnetization isotherm $M(H)$ curve at 5 K [Fig. 2(c)] shows typical behavior for type-II superconductivity. The lower critical field H_{c1} obtained from the M vs H plot at 5 K is 30 G [Fig. 2(d)]. The upper critical field $H_{c2} = 80$ kG at 26 K (with a slope of $dH/dT \sim -2.4$ T/K) has been estimated using field-dependent resistivity measurements [32] compared to the Pauli limit of $\mu_0 H_P = 18.4 T_c = 552$ kG (55.2 T) [33]. The specific heat as (C/T) is displayed in Fig. 2(e) for zero field and an applied field of 16 T. A clear anomaly is observed in a zero field corresponding to the superconducting transition at around 30 K, which is suppressed in the 16 T field. The jump in (C/T) at T_c was estimated by subtracting the 16 T data from that at the zero field, yielding a jump of $\Delta C/T_c = 25$ (mJ mol^{-1} K^{-2}), which is a factor of 2.78 larger than 9 (mJ mol^{-1} K^{-2}) observed in LaFeAsO and SmFeAsO polycrystalline samples [34]. To shed light on the nature of the gap symmetry, we also performed field-dependent heat-capacity measurements up to a field of 16 T. The field dependence of the specific heat coefficient $\gamma(H)$ was estimated by plotting C/T vs T^2 and extrapolating to $T \sim 0$ K and is displayed in Fig. 2(f). The estimated $\gamma(H)$ at $T \sim 0$ K exhibits a nonlinear magnetic-field dependence, but at 7 K it shows linear field dependence. The nonlinear behavior $\gamma(H) \sim H^{0.65}$, found in the low-temperature limit indicates the presence of nodal gap behavior. A very similar behavior of $\gamma(H) \sim H^{0.5}$ has been observed in $LaFeAsO_{0.9}F_{0.1}$ by Gang *et al.* [34] that has been attributed to the nodal gap structure.

Figures 3(a) and 3(b) show the TF-μSR precession signals above and below T_c obtained in the FC mode with an applied field of 400 G (well above $H_{c1} \sim 30$ G but below $H_{c2} \sim 80$ kG at 26 K). The observed decay of the μSR

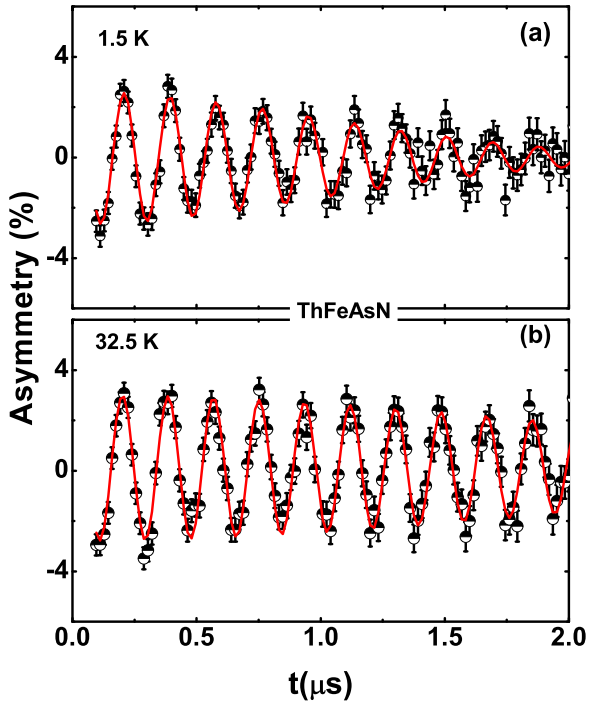

FIG. 3. Transverse-field μSR asymmetry spectra for ThFeAsN collected (a) at $T = 1.5$ K and (b) at $T = 32.5$ K (i.e., below and above T_c) in an applied magnetic field of $H = 400$ G. For the sake of clarity we present here the time-dependent asymmetry in the short-time region. The solid line shows a fit using Eq. (1).

signal with time below T_c is due to the inhomogeneous field distribution of the flux-line lattice. We have used an oscillatory decaying Gaussian function to fit the TF-μSR time-dependent asymmetry spectra, which is given below,

$$G_x(t) = A_1 \cos(2\pi \nu_1 t + \phi_1) \exp\left(\frac{-\sigma^2 t^2}{2}\right), \qquad (1)$$

where A_1 is the muon initial asymmetry, ν_1 is the frequency of the muon precession signal associated with the full volume of the sample, and ϕ_1 is the initial phase offset. The frequency associated with muon precession on hematite (on which the sample pellet was mounted) is very high (209 MHz or 15.48 kG) and is out of the time window of the MUSR spectrometer at the ISIS facility [35]. Furthermore, both the frequency and the relaxation rate of hematite are temperature independent below 100 K [35]. Equation (1) contains the total relaxation rate σ from the superconducting fraction of the sample; there are contributions from the vortex lattice (σ_{sc}) and nuclear dipole moments (σ_{nm}) where the latter is assumed to be constant over the entire temperature range [where $\sigma = \sqrt{(\sigma_{sc}^2 + \sigma_{nm}^2)}$]. The contribution from the vortex lattice σ_{sc} was determined by quadratically subtracting the background nuclear dipolar relaxation rate obtained from the spectra measured above T_c. As σ_{sc} is directly related to the superfluid density, it can be modeled by [36–38]

$$\frac{\sigma_{sc}(T)}{\sigma_{sc}(0)} = 1 + 2\left\langle \int_{\Delta_k}^{\infty} \frac{\partial f}{\partial E} \frac{E\,dE}{\sqrt{E^2 - \Delta_k^2}} \right\rangle_{\mathrm{FS}}, \qquad (2)$$

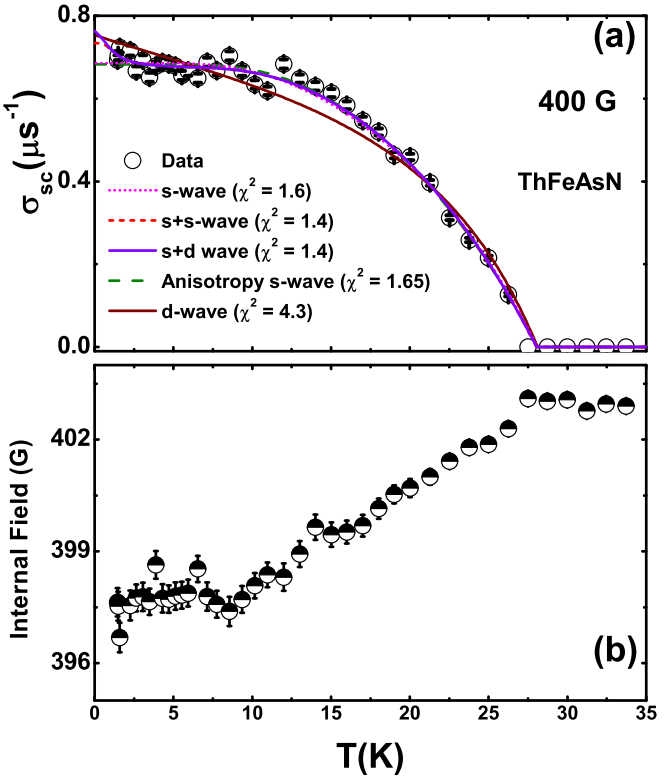

FIG. 4. (a) Temperature dependence of the muon depolarization rate $\sigma_{sc}(T)$ of ThFeAsN collected in an applied magnetic field of 400 G in a FC mode. $\sigma_{sc}(T)$ of the FC mode (symbols) where the lines are the fits to the data using Eq. (2) for various gap models. The dotted magenta line shows the fit using an isotropic single-gap s-wave model with $\Delta(0) = 5.1 \pm 0.1$ meV, the dashed red line and blue solid line show the fit to a two-gap model, the $s + s$ wave and $s + d$ wave, respectively, with $\Delta_1(0) = 5.2 \pm 0.1$ meV and $\Delta_2(0) = 0.3 \pm 0.1$ meV (for both models). The green long-dashed line shows the fit using an anisotropic s-wave model, and the solid purple line shows the fit using the d-wave model. (b) Temperature dependence of the internal field.

where $f = [1 + \exp(-E/k_BT)]^{-1}$ is the Fermi function and the brackets correspond to an average over the Fermi surface. The gap is given by $\Delta(T,\varphi) = \Delta_0 \delta(T/T_c) g(\varphi)$, whereas $g(\varphi)$'s refer to the angular dependence of the superconducting gap function, and φ is the azimuthal angle along the Fermi surface. We have used the BCS formula for the temperature dependence of the gap, which is given by $\delta(T/T_c) = \tanh\{(1.82)[1.018(T_c/T - 1)]^{0.51}\}$ [39]. $g(\varphi)$ [40,41] is given by (a) 1 for the s-wave gap [also for the $(s + s)$-wave gap], (b) $|\cos(2\varphi)|$ for the d-wave gap with line nodes, and (c) for the anisotropic s-wave model $\frac{|1+\cos(4\varphi)|}{2}$ [36,39,42,43].

Figure 4(a) shows the temperature dependence of σ_{sc}, measured in an applied field of 400 G collected in the FC mode. The FC mode is thermodynamically stable and provides direct information on the nature of the flux-line lattice. The temperature dependence of σ_{sc} increases with decreasing temperature confirming the presence of a flux-line lattice and indicates a decrease in the magnetic penetration depth ($\lambda^2 \sim \frac{1}{\sigma_{sc}}$) with decreasing temperature. The onset of diamagnetism below the superconducting transition can be seen through the decrease in the internal field below T_c as shown in Fig. 4(b). A small anomaly can be seen in the internal

TABLE I. Fitted parameters obtained from the fit to the $\sigma_{sc}(T)$ data of ThFeAsN using different gap models. The $T_c = 28.1 \pm 1$ K was estimated from the single isotropic s-wave gap fit and was kept fixed for fitting all the models.

Model	$g(\phi)$	Gap value $\Delta(0)$ (meV)	Gap ratio $2\Delta(0)/k_BT_c$	χ^2
s wave	1	5.1(1)	4.21	1.6
$s+s$ wave	1	5.2(1), 0.3(1)	4.29, 0.25	1.4
Anisotropy gap	$\frac{\lvert 1+\cos(4\phi)\rvert}{2}$	6.29	5.2	1.63
d wave	$\cos(2\phi)$	7.75	6.40	4.3
$s+d$ wave	1, $\cos(2\phi)$	5.2(1), 0.3(1)	4.29, 0.25	1.4

field below 10 K, and the origin of this is not clear at present. To find out whether this anomaly is due to any real phase transition in the vortex lattice below 10 K one needs detailed μSR measurements on single crystals of ThFeAsN for the muon beam both parallel and perpendicular to the c axis. From the analysis of the observed temperature dependence of σ_{sc} using different models for the gap, the nature of the superconducting gap can be probed. We have analyzed the temperature dependence of σ_{sc} based on five different models, the single-gap isotropic s-wave, the anisotropic s-wave, the line nodal d-wave models, the isotropic $(s+s)$-wave, and the $(s+d)$-wave two-gap models. The fits to the $\sigma_{sc}(T)$ data of ThFeAsN with various gap models using Eq. (2) are shown by lines (dashed, dotted, and solid) in Fig. 4(a), and the estimated fit parameters are given in Table I. It is clear from Fig. 4(a) that the d-wave model does not fit the data. On the other hand, the isotropic s-wave, the $(s+s)$-wave, the $(s+d)$-wave, and the anisotropic s-wave models show good fits to the $\sigma_{sc}(T)$ data. However, upon examining the agreement with the low-temperature upturn in the data, it is clear that only two models which explain this feature are the isotropic $(s+s)$-wave and $(s+d)$-wave two-gap models. Further support for the $(s+s)$- and $(s+d)$-wave models can be seen through the goodness of the fit χ^2 given in Table I. The value of $\chi^2 = 1.4$ for these models is the lowest. The estimated parameters for the $(s+s)$- and $(s+d)$-wave models show one larger gap of $\Delta_1(0) = 5.2 \pm 1$ (meV) and another much smaller gap of $\Delta_2(0) = 0.3 \pm 1$ (meV). The smaller gap is a nodal gap for the $(s+d)$-wave model. Our μSR analysis alone cannot distinguish between the $(s+s)$- and the $(s+d)$-wave models, but from combining the results with the field-dependent heat capacity, we conclude that the $(s+d)$-wave model is the best to explain the observed behavior of $\sigma_{sc}(T)$ and $\gamma(H)$. The value of $\sigma_{sc}(0) = 0.7637 \pm 3\ \mu s^{-1}$ was estimated from the $(s+d)$-wave fit while keeping $T_c = 28.1$ K fixed from the single isotropic s-wave gap fit. The estimated value of $2\Delta_1(0)/k_BT_c = 4.29 \pm 0.08$ from the $(s+s)$- and $(s+d)$-wave fits is comparable to that of the s-wave model (4.21) but larger than the value of 3.53 expected for BCS superconductors. On the other hand, for the smaller gap the value of $2\Delta_1(0)/k_BT_c = 0.25 \pm 0.08$ is much smaller than the BCS value. The two-gap nature, one larger and another smaller than the BCS value, are commonly observed in Fe-based superconductors [44] as well as in $Bi_4O_4S_3$ [45]. The multigap and d-wave order parameters are universal and intrinsic to cuprate superconductors [46,47], whereas Cr-based superconductors $A_2Cr_3As_3$ (A = K and Cs) exhibit a nodal gap [48,49]. Furthermore, the large value of $2\Delta_0/k_BT_c = 4.29 \pm 0.08$ indicates the presence of strong coupling and unconventional superconductivity in ThFeAsN. The two superconducting gaps (one larger and another smaller) also were observed in $SrFe_{1.85}Co_{0.15}As_2$ with $T_c = 19.2$ K in the scanning tunneling microscope study [50]. Moreover combined angle-resolved photoemission spectroscopy (ARPES) and μSR studies on $Ba_{1-x}K_xFe_2As_2$ with $T_c = 32.0$ K also reveal the presence of two gaps ($\Delta_1 = 9.1$ and $\Delta_2 = 1.5$ meV) [51].

The muon-spin depolarization rate (σ_{sc}) below T_c is related to the magnetic penetration depth (λ). For a triangular lattice [29,42,52], $\frac{\sigma_{sc}(T)^2}{\gamma_\mu^2} = \frac{0.00371\phi_0^2}{\lambda^4(T)}$, where $\gamma_\mu/2\pi = 135.5$ MHz/T is the muon gyromagnetic ratio and $\phi_0 = 2.07\times10^{-15}$ T m^2 is the flux quantum. This relation between σ_{sc} and λ is valid for $0.13/\kappa^2 \ll (H/H_{c2}) \ll 1$, where $\kappa = \lambda/\xi \gg 70$ [53]. As with other phenomenological parameters characterizing a superconducting state, the penetration depth can also be related to microscopic quantities. Using London theory [29], $\lambda_L^2 = m^*c^2/4\pi n_s e^2$, where $m^* = (1+\lambda_{e\text{-}ph})m_e$ is the effective mass and n_s is the density of superconducting carriers. Within this simple picture, λ_L is independent of the magnetic field. $\lambda_{e\text{-}ph}$ is the electron-phonon coupling constant, which can be estimated from Θ_D and T_c using McMillan's relation [54] $\lambda_{e\text{-}ph} = \frac{1.04+\mu^*\ln(\Theta_D/1.45T_c)}{(1-0.62\mu^*)\ln(\Theta_D/1.45T_c)+1.04}$, where μ^* is the repulsive screened Coulomb parameter and usually assigned as $\mu^* = 0.13$. For ThFeAsN, we have used $T_c = 28.1$ K and $\Theta_D = 332$ K [27], which together with $\mu^* = 0.13$, we have estimated $\lambda_{e\text{-}ph} = 1.48$. Furthermore, assuming that roughly all the normal state carriers (n_e) contribute to the superconductivity (i.e., $n_s \approx n_e$), we have estimated the magnetic penetration depth λ, superconducting carrier density n_s, and effective-mass enhancement m^* to be $\lambda_L(0) = 375$ nm [from the $(s+d)$-wave fit], $n_s = 4.97\times10^{27}$ carriers/m^3, and $m^* = 2.48m_e$, respectively.

The correlation between T_c and σ_{sc} observed in μSR studies has suggested a new empirical framework for classifying superconducting materials [55]. Here we explore the role of muon-spin relaxation rate/penetration depth in the superconducting state for the characterization and classification of superconducting materials as first proposed by Uemura *et al.* [55]. In particular we focus upon the classification scheme of Uemura *et al.* [55] which considers the correlation between the superconducting transition temperature T_c and the effective Fermi temperature T_F determined from μSR measurements of the penetration depth [56]. Within this scheme strongly correlated exotic superconductors, i.e., high-T_c cuprates, heavy fermions, Chevrel phases, and the organic superconductors form a common but distinct group, characterized by a universal scaling of T_c with T_F such that $1/10 > (T_C/T_F) > 1/100$ (Fig. 5). For conventional BCS superconductors, $1/1000 > (T_c/T_F)$. Considering the value of $T_c/T_F = 30/4969.4 = 0.006$ for ThFeAsN (see Fig. 5), this material can be classified as not an exotic superconductor but very close to this limit according to the classification of Uemura *et al.* [55].

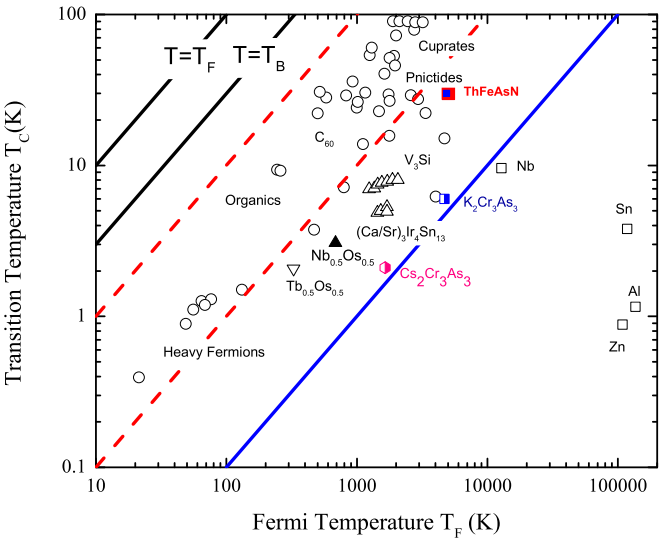

FIG. 5. A schematic of the plot of Uemura *et al.* [55] of superconducting transition temperature T_c against effective Fermi temperature T_F. The big solid red square and small blue square (on top of the red square) show the points calculated using the $(s+d)$- and $(s+s)$-wave models, respectively, for ThFeAsN. The "exotic" superconductors fall within a common band for which $1/100 < T_c/T_F < 1/10$, indicated by the region between two red color dashed lines in the figure. The solid black line corresponds to the Bose-Einstein condensation temperature (T_B) [56].

IV. CONCLUSIONS

In conclusion, we have presented the resistivity, magnetization, heat capacity, and TF-μSR measurements in the normal and superconducting states of ThFeAsN, which have tetragonal layered crystal structures. Our magnetization and heat-capacity measurements confirmed the bulk superconductivity with $T_c = 30$ K. From the TF-μSR we have determined the muon depolarization rate in the FC mode associated with the vortex lattice. The temperature dependence of σ_{sc} fits better to a two-gap model with either an isotropic $s+s$ wave or a $s+d$ wave than a single-gap isotropic s-wave, anisotropic s-wave, or d-wave models. Our μSR analysis alone cannot distinguish between the $(s+s)$- and the $(s+d)$-wave models, but combining the results with field-dependent heat capacity, we conclude that the $(s+d)$-wave model is the best to explain the observed behavior of $\sigma_{sc}(T)$ and $\gamma(H)$. Furthermore, the value (for the larger gap) of $2\Delta_1(0)/k_BT_c = 4.29 \pm 0.08$ obtained from the $(s+s)$- and $(s+d)$-wave gap models fit is larger than 3.53, expected for BCS superconductors, indicating the presence of strong-coupling superconductivity in ThFeAsN. Moreover, two superconducting gaps have also been observed in the Fe-based families of superconductors, and hence our observation of two gaps is in agreement with the general trend observed in Fe-based superconductors. Further confirmation of the presence of two gaps in ThFeAsN would require ARPES studies on single crystals of ThFeAsN. The present results will help to develop a realistic theoretical model to understand the origin of superconductivity in ThFeAsN.

ACKNOWLEDGMENTS

D.A. and H.L. would like to thank the Royal Society of London for the U.K.-China Newton funding. D.A. and A.H. would like to thank CMPC-STFC, Grant No. CMPC-09108, for financial support. A.B. would like to acknowledge DST India for an Inspire Faculty Research Grant and ISIS-STFC for funding support. The work at IOP, CAS was supported by the National Natural Science Foundation of China (Grants No. NSFC-11374011 and No. 11611130165) and the Strategic Priority Research Program (B) of the Chinese Academy of Sciences (Grants No. XDB07020300 and No. XDPB01). H.L. would like to acknowledge support from the Youth Innovation Promotion Association of CAS (Grant No. 2016004). We would like to thank Dr A. Hannon for help with the CRYSTALMAKER software.

[1] J. Bardeen, L. N. Cooper, and J. R. Schrieffer, Phys. Rev. **106**, 162 (1957).
[2] J. Paglione and R. L. Greene, Nat. Phys. **6**, 642 (2010).
[3] G. R. Stewart, Adv. Phys. **66**, 75 (2017).
[4] P. Dai, H. A. Mook, S. M. Hayden, G. Aeppli, T. G. Perring, R. D. Hunt, and F. Dogan, Science **284**, 1344 (1999).
[5] P. Dai, Rev. Mod. Phys. **87**, 855 (2015).
[6] M. P. Allan, F. Massee, D. K. Morr, J. Van Dyke, A. W. Rost, A. P. Mackenzie, C. Petrovic, and J. C. Davis, Nat. Phys. **9**, 468 (2013).
[7] C. de la Cruz *et al.*, Nature (London) **453**, 899 (2008).
[8] Q. Huang, J. Zhao, J. W. Lynn, G. F. Chen, J. L. Luo, N. L. Wang, and P. C. Dai, Phys. Rev. B **78**, 054529 (2008).
[9] T. Shibauchi, A. Carrington, and Y. Matsuda, Annu. Rev. Condens. Matter Phys. **5**, 113 (2014).
[10] D. R. Parker, M. J. P. Smith, T. Lancaster, A. J. Steele, I. Franke, P. J. Baker, F. L. Pratt, M. J. Pitcher, S. J. Blundell, and S. J. Clarke, Phys. Rev. Lett. **104**, 057007 (2010).
[11] T. J. Liu *et al.*, Nat. Mater. **9**, 716 (2010).
[12] N. Katayama *et al.*, J. Phys. Soc. Jpn. **79**, 113702 (2010).
[13] N. Katayama *et al.*, J. Phys. Soc. Jpn. **82**, 123702 (2013).
[14] S. Jiang, L. Liu, M. Schütt, A. M. Hallas, B. Shen, W. Tian, E. Emmanouilidou, A. Shi, G. M. Luke, Y. J. Uemura, R. M. Fernandes, and N. Ni, Phys. Rev. B **93**, 174513 (2016).
[15] Z.-Z.-A. Ren, G.-C. Che, X.-L. Dong, J. Yang, W. Lu, W. Yi, X.-L. Shen, Z.-C. Li, L.-L. Sun, F. Zhou, and Z.-X. Zhao, Europhys. Lett. **83**, 17002 (2008).
[16] X. C. Wang, Q. Q. Liu, Y. X. Lv, W. B. Gao, L. X. Yang, R. C. Yu, F. Y. Li, and C. Q. Jin, Solid State Commun. **148**, 538 (2008).
[17] S. Matsuishi, Y. Inoue, T. Nomura, H. Yanagi, M. Hirano, and H. Hosono, J. Am. Chem. Soc. **130**, 14428 (2008).
[18] X. Y. Zhu, F. Han, P. Cheng, G. Mu, B. Shen, and H.-H. Wen, Europhys. Lett. **85**, 17011 (2009).
[19] S. Iimura *et al.*, Nat. Commun. **3**, 943 (2012).
[20] M. Hiraishi *et al.*, Nat. Phys. **10**, 300 (2014).
[21] C. Wang, Z. C. Wang, Y. M. Mei, Y. K. Li, L. Li, Z. T. Tang, Y. Liu, P. Zhang, H. F. Zhai, Z. A. Xu, and G. H. Cao, J. Am. Chem. Soc. **138**, 2170 (2016).

[22] Z. C. Wang, C. Y. He, S. Q. Wu *et al.*, J. Am. Chem. Soc. **138**, 7856 (2016).
[23] Z. C. Wang, C. Y. He, Z. T. Tang, S. Q. Wu, and G. H. Cao, Sci. China Mater. **60**, 83 (2017).
[24] D. J. Singh, J. Alloys Compd. **687**, 786 (2016).
[25] G. Wang and X. Shi, Europhys. Lett. **113**, 67006 (2016).
[26] H. Mao, C. Wang, H. E. Maynard-Casely, Q. Huang, Z. Wang, G. Cao, S. Li, and H. Luo, Europhys. Lett. **117**, 57005 (2017).
[27] M. A. Albedah *et al.*, J. Alloys Compd. **695**, 1128 (2017).
[28] S. L. Lee, S. H. Kilcoyne, and R. Cywinski, *Muon Science: Muons in Physics, Chemistry and Materials* (SUSSP-IOP, Bristol, 1999).
[29] J. E. Sonier, J. H. Brewer, and R. F. Kiefl, Rev. Mod. Phys. **72**, 769 (2000).
[30] F. L. Pratt, Physica B (Amsterdam) **289-290**, 710 (2000).
[31] Y. Kamihara, T. Watanabe, M. Hirano, and H. Hosono, J. Am. Chem. Soc. **130**, 3296 (2008).
[32] G. H. Cao (private communication).
[33] A. M. Clogston, Phys. Rev. Lett. **9**, 266 (1962).
[34] M. U. Gang, Z. Xi-Yu, F. Lei, S. Lei, R. Cong, and W. Hai-Hu, Chin. Phys. Lett. **25**, 2221 (2008).
[35] K. Ruegg, C. Boekema, A. Denison, W. Hofmann, and W. Kunding, J. Magn. Magn. Mater. **15**, 669 (1980).
[36] R. Prozorov and R. W. Giannetta, Supercond. Sci. Technol. **19**, R41 (2006).
[37] A. Bhattacharyya, D. T. Adroja, J. Quintanilla, A. D. Hillier, N. Kase, A. M. Strydom, and J. Akimitsu, Phys. Rev. B **91**, 060503(R) (2015).
[38] A. Bhattacharyya, D. T. Adroja, N. Kase, A. D. Hillier, J. Akimitsu, and A. M. Strydom, Sci. Rep. **5**, 12926 (2015).
[39] A. Carrington and F. Manzano, Physica C (Amsterdam) **385**, 205 (2003).
[40] J. F. Annett, Adv. Phys. **39**, 83 (1990).
[41] G. M. Pang, M. Smidman, W. B. Jiang, J. K. Bao, Z. F. Weng, Y. F. Wang, L. Jiao, J. L. Zhang, G. H. Cao, and H. Q. Yuan, Phys. Rev. B **91**, 220502(R) (2015).
[42] E. E. M. Chia, M. B. Salamon, H. Sugawara, H. Sato, Phys. Rev. B **69**, 180509(R) (2004).
[43] A. Bhattacharyya, D. T. Adroja, A. D. Hillier, R. Jha, V. P. S. Awana, and A. M. Strydom, J. Phys.: Condens. Matter **29**, 265602 (2017).
[44] D. V. Evtushinsky, D. S. Inosov, V. B. Zabolotnyy, M. S. Viazovska, R. Khasanov, A. Amato, H.-H. Klauss, H. Luetkens, Ch. Niedermayer, G. L. Sun, V. Hinkov, C. T. Lin, A. Varykhalov, A. Koitzsch, M. Knupfer, B. Büchner, A. A. Kordyuk, and S. V. Borisenko, New J. Phys. **11**, 055069 (2009).
[45] P. K. Biswas, A. Amato, C. Baines, R. Khasanov, H. Luetkens, H. Lei, C. Petrovic, and E. Morenzoni, Phys. Rev. B **88**, 224515 (2013).
[46] R. Khasanov, S. Strassle, D. Di Castro, T. Masui, S. Miyasaka, S. Tajima, A. Bussmann-Holder, and H. Keller, Phys. Rev. Lett. **99**, 237601 (2007).
[47] B. Keimer, S. A. Kivelson, M. R. Norman, S. Uchida, and J. Zaanen, Nature (London) **518**, 179 (2015).
[48] D. T. Adroja, A. Bhattacharyya, M. Smidman, A. Hillier, Y. Feng, B. Pan, J. Zhao, M. R. Lees, A. Strydom, and P. K. Biswas, J. Phys. Soc. Jpn. **86**, 044710 (2017).
[49] D. T. Adroja, A. Bhattacharyya, M. Telling, Yu. Feng, M. Smidman, B. Pan, J. Zhao, A. D. Hillier, F. L. Pratt, and A. M. Strydom, Phys. Rev. B **92**, 134505 (2015).
[50] Y. Bang and G. R. Stewart, J. Phys.: Condens. Matter **29**, 123003 (2017).
[51] R. Khasanov, D. V. Evtushinsky, A. Amato, H.-H. Klauss, H. Luetkens, C. Niedermayer, B. Büchner, G. L. Sun, C. T. Lin, J. T. Park, D. S. Inosov, and V. Hinkov, Phys. Rev. Lett. **102**, 187005 (2009).
[52] See, for example, A. Amato, Rev. Mod. Phys. **69**, 1119 (1997).
[53] E. H. Brandt, Phys. Rev. B **68**, 054506 (2003).
[54] W. McMillan, Phys. Rev. **167**, 331 (1968).
[55] Y. J. Uemura, G. M. Loke, B. J. Sternlieb, J. H. Brewer, J. F. Carolan, W. N. Hardy, R. Kadono, J. R. Kempton, R. F. Kiefl, S. R. Kreitzman, P. Mulhern, T. M. Riseman, D. Ll. Williams, B. X. Yang, S. Uchida, H. Takagi, J. Gopalkrishnan, A. W. Sleight, M. A. Subramanian, C. L. Chien, M. Z. Cieplak, G. Xiao, V. Y. Lee, B. W. Statt, C. E. Stronach, W. J. Kossler, and X. H. Yu, Phys. Rev. Lett. **62**, 2317 (1989).
[56] A. H. Hillier and R. Cywinski, Appl. Magn. Reson. **13**, 95 (1997).